Comparative PMTs Charge Response of Water and Water-based Liquid Scintillator for Next-Generation Neutrino Experiments

Xiaoyan Fan
Department of Physics, University of Malaya

Yokoyama-Nakajima Group, Department of Physics, University of Tokyo

September 18, 2025

Abstract

The water-based liquid scintillator (WbLS) has emerged as a promising detection medium for next-generation neutrino experiments, combining the directional sensitivity of Cherenkov light from pure water with the high light yield of scintillation. In this study, the relative light yields of pure water and a WbLS mixture were compared using integrated charge from photomuliplier tubes(PMTs). Measurements were performed under identical conditions with cosmic muons as the light source. The WbLS sample exhibited a significantly higher integrated charge compared to pure water, consistent with the expected scintillation contribution.

1 Introduction

1.1 Neutrino Detection and the Role of Detection Media

Neutrinos are fundamental particles that interact only through weak nuclear force and gravity, making their detection inherently challenging. Despite their elusive nature, neutrinos play a crucial role in understanding astrophysical phenomena, fundamental particle properties, and physics beyond the Standard Model. Large-scale neutrino detectors are therefore designed to maximize the probability of neutrino interactions and to identify their rare signatures with high precision.

The choice of detection medium is a key factor in determining the sensitivity, resolution, and cost-effectiveness of a neutrino detector. Water Cherenkov detectors, such as Super-Kamiokande(Fukuda et al., 2003), utilize the emission of Cherenkov photons by relativistic charged particles traveling faster than the phase velocity of light in water. These detectors are well-established for their scalability and directional reconstruction capabilities. Liquid scintillator detectors, such as JUNO(An et al., 2016), employ organic scintillators to produce isotropic scintillation light, offering higher light yield and superior energy resolution compared to pure water.

In recent years, hybrid detection media such as water-based liquid scintillator (WbLS) have emerged as promising candidates for next-generation neutrino experiments(Xiang et al., 2024). By combining the directional sensitivity of Cherenkov radiation with the high light yield of scintillation, WbLS aims to improve particle identification, energy resolution, and sensitivity to low-energy neutrinos, while maintaining the scalability and cost advantages of water-based systems. As such, the optimization and characterization of detection media remain central to the advancement of neutrino physics.

1.2 Water-based Liquid Scintillator (WbLS)

The water-based liquid scintillator (WbLS) is a novel detection medium that combines the properties of pure water and organic liquid scintillators through stable emulsification(Yeh et al., 2011). Typically, WbLS consists of a majority fraction of water mixed with an organic scintillating component such as linear alkylbenzene (LAB), along with surfactants to ensure optical stability. In this hybrid medium, two distinct light production mechanisms coexist: Cherenkov radiation from relativistic charged particles and scintillation light from the organic component.

The key advantages of WbLS stem from this unique combination(Onda et al., 2025). Firstly, the ratio of Cherenkov to scintillation light can be tuned by adjusting the scintillator concentration,

allowing flexible optimization of the detector response for different physics goals. Secondly, the additional scintillation photons significantly enhance the energy resolution and lower the detection threshold, improving the sensitivity to low-energy neutrino events. Moreover, the distinct timing profiles of Cherenkov and scintillation light enable particle identification capabilities by differentiating prompt Cherenkov signals from delayed scintillation photons. Finally, unlike pure liquid scintillators, WbLS exhibits compatibility with metal loading, such as gadolinium doping, which is valuable for neutron capture and background suppression.

In addition to these performance benefits, WbLS retains many practical advantages of traditional water Cherenkov detectors, including low cost, ease of handling, and scalability to kiloton-scale volumes. This combination makes WbLS particularly attractive for next-generation neutrino experiments that require both high sensitivity to low-energy events and precise reconstruction of complex event topologies.

Therefore, a comprehensive characterization of WbLS under controlled laboratory conditions—including measurements of light yield, optical properties, and detector response—is essential to guide its implementation in large-scale neutrino detectors. This study is motivated by the need to deepen the understanding and optimize the performance of WbLS to support future experimental applications. Specifically, this work focuses on the quantitative analysis of detector response, represented by the integral of ADC signals from PMTs as raw data.

2 Methodology

2.1 Experimental Setup

The experimental setup(see Fig. 1, 2, 3) was designed to characterize the optical response of the WbLS to cosmic muons. The WbLS sample was contained in a rectangular acrylic tank with dimensions of 160 mm × 110 mm × 50 mm, providing a compact but well-defined detection volume. The plastic scintillator (PS) was placed adjacent to the tank and optically coupled to the trigger photomultiplier tube (T-PMT) using optical grease to ensure efficient light transmission and minimize reflection losses at the interface. The T-PMT(Hamamatsu H7195) detected scintillation light produced when cosmic muons passed through the PS, generating a fast trigger signal. This trigger was used to gate the data acquisition system and synchronize the readout of the main PMT,

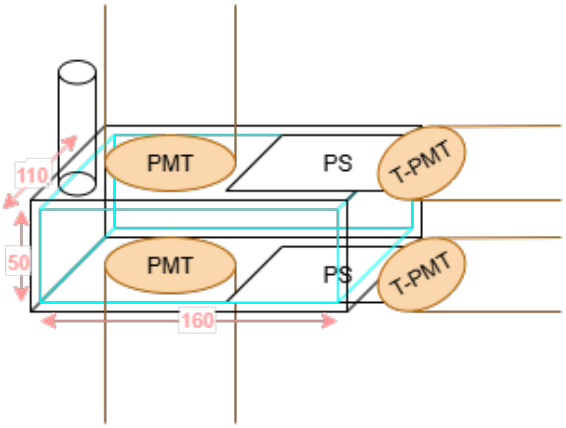

Figure 1: Schematic illustration of the configuration.

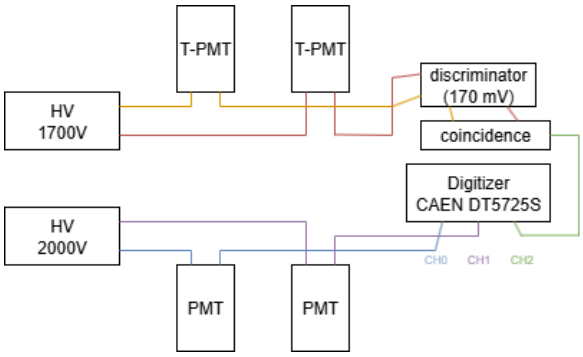

Figure 2: Schematic illustration of the circuit.

which was attached directly in the WbLS volume to capture Cherenkov and scintillation light. The main PMT (Hamamatsu H7195) was oriented to maximize light collection efficiency and was operated by coincidence with the trigger system to select only events induced by cosmic muons. All optical interfaces were coupled with optical grease to reduce refractive index mismatch and enhance photon collection. The waveform signals from both PMTs were recorded using a fast digitizer(CAEN DT5725S) with 250 MSa/s sampling rate, allowing detailed pulse shape analysis. Although the current analysis is based on raw ADC counts, future work will include energy calibration using radioactive sources to convert the measured signals into absolute photoelectron yield. This setup enables a direct comparison of light output between WbLS and pure water under identical detection conditions, serving as a testbed for optimizing WbLS formulations for next-generation neutrino and rare-event detectors.

2.2 Scintillator Samples

The scintillator samples(Tab.1) used in this study were prepared using a two-step procedure. First,

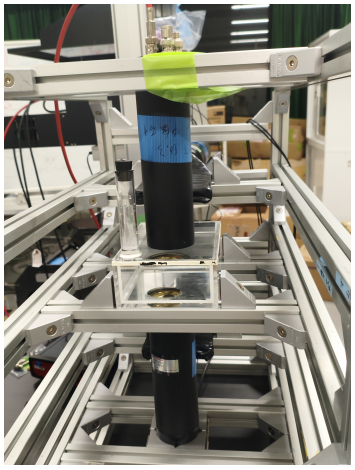

Figure 3: Photograph of the actual setup.

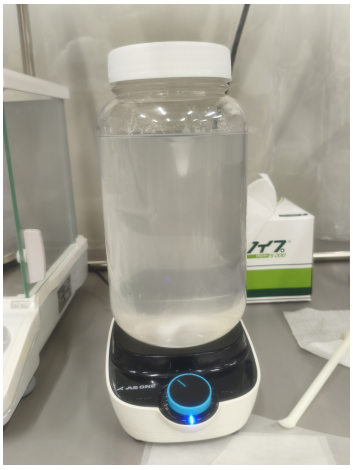

Figure 4: Preparation process of the WbLS sample. The scintillator cocktail was first premixed, followed by emulsification with the aqueous phase using a magnetic stirrer for homogeneous mixing.

Table 1: Mass composition of the WbLS sample, normalized to a total mass of 100 g.

Component	Target Mass	Measured Mass
Water	88.000g	88.043g
LAB (Linear Alkylbenzene)	10.000g	10.940g
Triton X-100	1.000g	1.015g
PPO (2,5-Diphenyloxazole)	1.00mg	1.04mg
9-Methylcarbazole	30μg	30μg

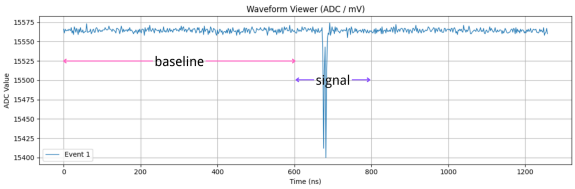

Figure 5: Example of a recorded waveform showing the baseline and signal regions. The baseline is determined by averaging the ADC values within the 0–600 ns interval, and the signal region is defined as 600–800 ns, where the integrated charge is calculated.

a scintillator cocktail was formulated by dissolving 2,5-diphenyloxazole (PPO) and methylcarbazole in linear alkylbenzene (LAB). LAB serves as the organic solvent and primary energy transfer medium, offering high optical transparency and chemical stability. PPO acts as the primary fluor, converting the energy deposited by charged particles into ultraviolet and visible photons with high efficiency. Methylcarbazole is added as a secondary wavelength shifter, which extends the emission spectrum and improves the compatibility of scintillation light with the spectral response of the photodetector(Díaz et al., 2001).

In the second step, a small aliquot of the prepared scintillator cocktail was introduced into a water-based mixture containing Triton X-100 and LAB(See Fig.4). TX-100 functions as a nonionic surfactant, enabling stable emulsification between the hydrophobic LAB and the aqueous phase, thereby maintaining the long-term optical stability of the WbLS. The final sample thus incorporates both Cherenkov and scintillation light production mechanisms within a homogeneous and optically stable medium, suitable for subsequent detector response measurements.

3 Data Analysis

Using this set-up, the detection rate of cosmic muons was measured to be approximately 9,300 events per 24 hours. Based on this rate, subsequent experimental runs were conducted with durations of 10 and 20 hours. The 10-hour runs were used for comparative studies of muon direction determination, while the 20-hour runs were dedicated to comparing the light yield and initial waveform characteristics between WbLS and pure water. This allocation of run times was chosen to ensure sufficient statistical significance for each analysis objective while balancing the data collection efficiency and the stability requirements of the experimental setup.

3.1 Signal Waveform Analysis

Waveform analysis begins by establishing a baseline level, which is calculated as the average ADC value over the initial 0 to 600 ns period - during which no physical signal is expected(see Fig. 5).

This baseline is then subtracted from the entire waveform to correct for electronic noise.

The signal window is defined according to the post-trigger position of the DAQ board, which has been configured at 50% of the total acquisition length, corresponding to 630 ns. 600 to 800 ns is used for signal integration. This window captures the region where the physical pulse appears above the baseline. The sum of the integrated ADC difference within this interval serves as a measure of the detected charge for subsequent quantitative analysis.

3.2 Relative Light Yield (ADC Counts)

Some events appear to be missing or not properly recorded. The primary cause is a geometric mismatch between the plastic trigger scintillator and the water tank, resulting in incomplete coverage of the area above the tank(see Fig. 6). Consequently, certain cosmic muons may traverse the trigger scintillator without entering the tank, causing the main PMTs to record no signal.

Such events contribute noise to the dataset, lowering the mean light yield. To address this, a data selection cut was applied. The method involves plotting the *signal depth* versus the *integrated area* for all recorded events (see Fig. 7). As expected, events with integrated area values near zero cluster symmetrically around the vertical axis, indicating a lack of correlated PMT signal. Events with a signal depth within the range of 0–10 ADC counts and an integrated area between –150 and 150 ADC counts were excluded from the final analysis to obtain a more accurate estimate of the relative light yield.

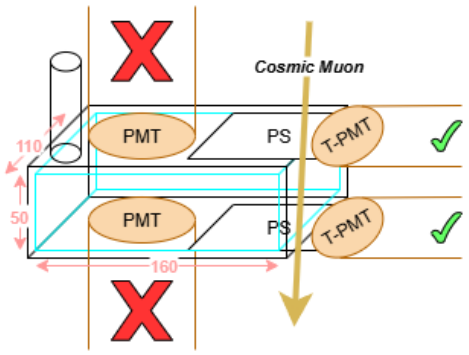

Figure 6: The main reason of missing events - Geometric mismatch

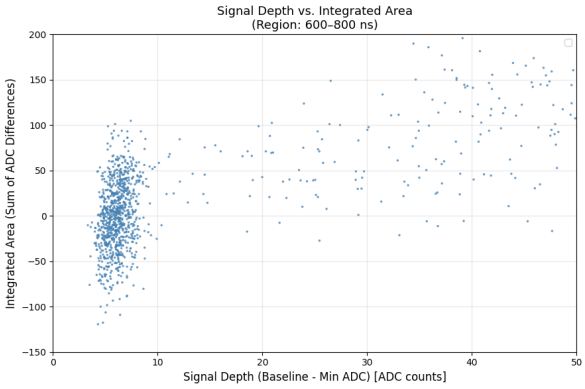

Figure 7: Scatter plot of signal depth vs. integrated area. Events clustering near zero integrated area correspond to noise or mismatched triggers, which are removed in the analysis.

4 Results

4.1 Signal Waveform

Qualitatively, the WbLS waveforms exhibit a longer tail and, in some cases, a clearly resolved double-peak structure, which enables the separation of scintillation light from the prompt Cherenkov component. In contrast, the waveforms recorded with pure water show a sharp, single peak without a discernible tail.

Quantitatively, a peak-finding algorithm was applied in the 640–720 ns region, using a local baseline comparison to identify possible secondary peaks. The analysis reveals that the fraction of double-peak events is **2.9%** for water and **5.3%** for WbLS. As illustrated in Fig. 8, the double-peak events identified in water are typically single-peaked waveforms with minor fluctuations misidentified as secondary peaks, whereas the double-peak events in WbLS correspond to a genuine temporal separation between the Cherenkov and scintillation components(See Fig.9).

These results demonstrate that WbLS provides enhanced time profile discrimination compared to pure water, allowing a more effective distinction between prompt and delayed light signals.

4.2 Cosmic Muon Direction

The directional response test was conducted under pure water conditions, with an applied voltage of 1700 V, to avoid complications from scintillation light. The two PMTs used in this study were not gain-calibrated; therefore, their raw ADC values cannot be directly converted into absolute photon counts. To eliminate the influence of inter-PMT gain differences, a position-swapping method was applied. Each PMT was alternately placed at the

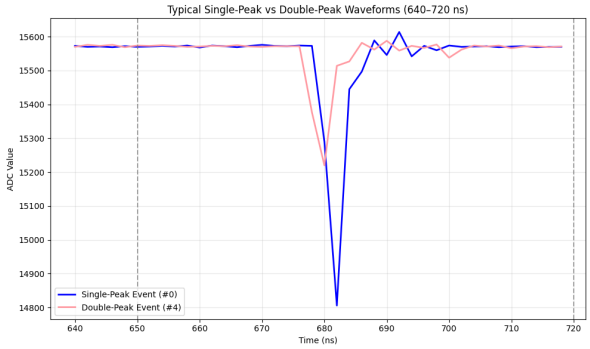

Figure 8: Example single-peak and double-peak waveforms recorded in pure water. The single-peak waveform exhibits a sharp profile without a discernible tail, while the double-peak case shown here is a misidentification caused by baseline fluctuations.

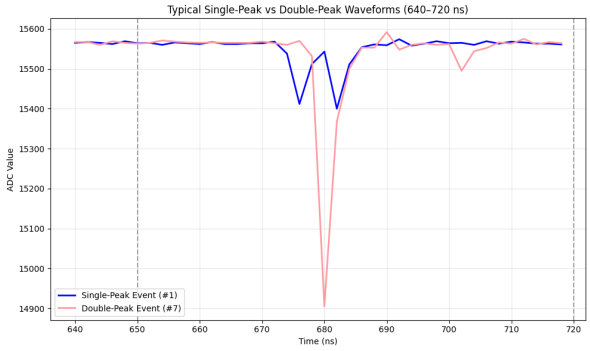

Figure 9: Example single-peak and double-peak waveforms recorded in WbLS. The double-peak waveform clearly exhibits temporal separation between the prompt Cherenkov light and the delayed scintillation component.

top and bottom positions of the detector, enabling a comparison of the same PMT's response at different positions.

For clarity, the PMTs are denoted as PMT-A and PMT-B, where PMT-A(top) and PMT-B(bottom) represent the initial configuration, and PMT-A(bottom) and PMT-B(top) represent the configuration after swapping positions.

The measured mean integrated ADC counts, calculated from the cut-processed raw data, are as follows:

- PMT-A(top): 131.08 ± 2.25
- PMT-A(bottom): 151.71 ± 4.07
- PMT-B(top): 387.26 ± 5.57
- PMT-B(bottom): 504.20 ± 16.27

The results indicate that the PMT located at the bottom position consistently records a higher signal compared to the same PMT when placed at the top position. This is consistent with the expected predominance of downward-going cosmic muons. In contrast, the light detected by the upper PMT primarily originates from reflections within the tank, resulting in a lower overall signal. As shown in Fig. 10, the response of PMT-A demonstrates a clear dependence on its vertical position. Additional distributions for PMT-B are provided in Appendix A.

4.3 Comparative Light Yield in Water and WbLS

The relative light yield was evaluated by integrating the ADC counts over the signal window after baseline subtraction. Measurements were performed for two photomultiplier tubes (PMTs) positioned at the top and bottom of the detector, operated at a working voltage of 2000 V, with selection efficiencies applied to remove noise-dominated events.

The measured mean integrated ADC counts, calculated from the cut-processed raw data, are as follows:

- PMT-A:WbLS(top): 758.43 ± 39.20
- PMT-B:WbLS(bottom): 1529.74 ± 9.27
- PMT-A:Water(top): 589.10 ± 15.23
- PMT-B:Water(bottom): 1421.78 ± 15.66

This corresponds to a relative increase of approximately +28.74% for the top PMT and +7.59% for the bottom PMT when using WbLS instead of water. Since scintillation photons are

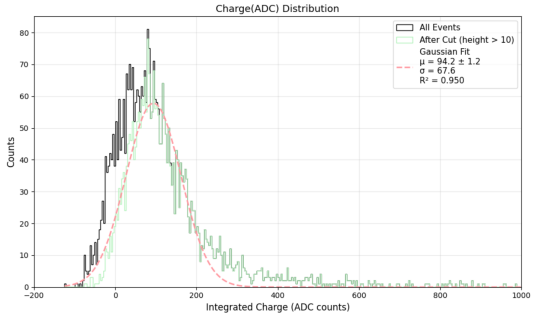

(a) PMT-A at the top position

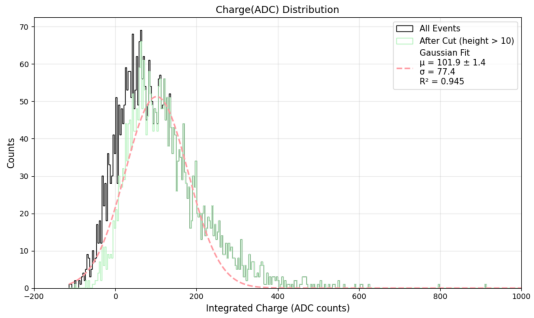

(b) PMT-A at the bottom position

Figure 10: Integrated ADC distributions for PMT-A under different positional configurations in pure water. Panel (a) shows PMT-A at the top position, while panel (b) shows PMT-A at the bottom position.

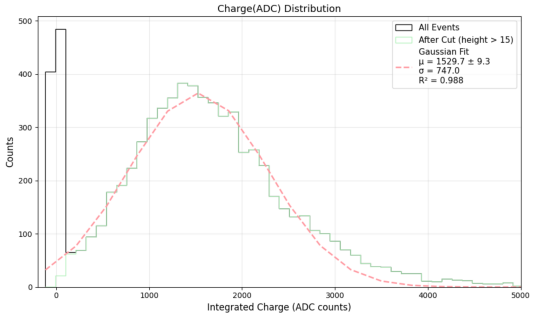

(a) WbLS

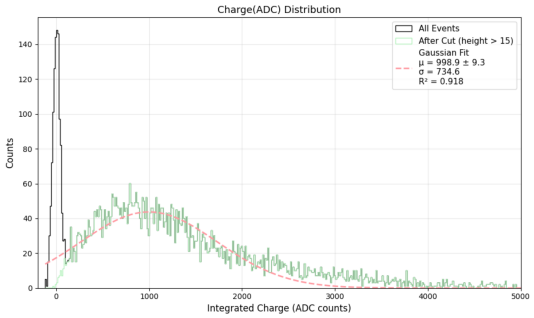

(b) Pure Water

Figure 11: Integrated ADC distributions for WbLS and pure water. Panel (a) corresponds to PMT-B at the bottom position in WbLS, whereas panel (b) shows the same configuration with pure water.

produced isotropically, both PMTs are expected to receive a similar absolute amount of additional light. However, because the top PMT initially collects less Cherenkov light due to the directional nature of Cherenkov emission, the relative contribution of the added scintillation component becomes larger for the top PMT. This behavior is consistent with the expectation that the relative increase should be more pronounced at the top.

Figure 11 shows the distributions of integrated ADC counts for WbLS and water. Gaussian fits are displayed in the figure as a visual guide, but the quantitative comparison and the reported increase percentages are based on the raw data mean values. Additional distributions for Top-PMTs comparison are provided in Appendix B.

5 Limitations and Future Work

Several limitations of the present study should be noted. First, the PMTs were not calibrated to absolute photon counts, which prevents direct determination of the true light yield. Second, due to limited experimental time, only a single WbLS composition was investigated, and variations in the concentration of Methylcarbazole were not explored. Consequently, the potential impact of different scintillator loadings on light yield and waveform characteristics remains unquantified. Third, this work focused primarily on integrated ADC counts, and other optical properties of WbLS, such as attenuation length, scattering, and timing characteristics, were not systematically measured or compared with pure water.

Future studies will aim to address these limitations. Absolute PMT calibration will enable direct photon yield determination. Systematic investigation of WbLS samples with varying scintillator fractions, including different Methylcarbazole concentrations, will provide a more comprehensive understanding of the tunable light output. Additionally, detailed studies of other optical parameters will help optimize WbLS performance for neutrino detection and enable more accurate modeling of detector response.

Despite these limitations, WbLS demonstrates clear advantages over pure water in terms of combined Cherenkov and scintillation light yield and time-profile discrimination capabilities. Further optimization of WbLS composition and detailed optical characterization can enhance its potential for next-generation neutrino experiments and other applications requiring high light collection efficiency and precise timing information.

6 Conclusion

A comparative study of pure water and water-based liquid scintillator (WbLS) has been carried out using a small-scale detector equipped with four photomultiplier tubes. The results confirm that WbLS enhances both light collection and temporal signal characteristics relative to pure water.

Time-profile analysis shows that WbLS waveforms exhibit longer tails and a larger fraction of double-peak events, indicating the presence of distinct Cherenkov and scintillation components. In contrast, pure water produces sharp single-peak signals with negligible tails. Quantitatively, the mean integrated ADC counts are higher for WbLS, with relative increases of approximately +28.74% at the top PMT and +7.59% at the bottom PMT. This trend is consistent with expectations: because the top PMT receives less Cherenkov light due to its directional nature, the relative contribution of isotropic scintillation photons is correspondingly larger.

Cosmic muon direction studies further confirm the geometric expectation that the bottom PMT registers a higher absolute light yield than the top PMT, independently of PMT swapping.

In summary, WbLS demonstrates clear improvements in both light yield and time-based signal separation compared to pure water. The observed consistency with physical expectations strengthens the case for WbLS as a tunable detection medium. Future work should include systematic calibration of absolute photon yield and exploration of different WbLS compositions to fully evaluate its potential for next-generation neutrino experiments.

7 Acknowledgment

The author expresses sincere gratitude to Professor Yasuhiro Nakajima for his meticulous academic guidance. Special thanks are extended for the opportunity to visit the Super-Kamiokande detector on July 29, coincidentally falling exactly two years after the first time the author became aware of and fascinated by Super-Kamiokande on July 29, 2022.

Gratitude is extended to the UTRIP Office of the School of Science, University of Tokyo, for their recognition and support, and to Kono Kuniko for assistance with reimbursement procedures. The author is also grateful to Daiwa Securities Company for their generous financial support. Sincere thanks go to senior colleagues in the office, including Yota Endo, Tomochika Arai, Shoma Kodama, and others, whose guidance and kindness were invaluable, as well as to the small treats in the office (Pino and Senbei) that brightened the days. Special appreciation is given to fellow interns, Peter, Aaryan, and others, not only for being wonderful roommates, but also for the shared laughter and encouragement throughout the stay in Tokyo. Finally, heartfelt thanks are owed to the author's girlfriend and parents for their unwavering moral support.

Figure 12: Super-Kanmiokande

Appendix

A Additional Charge Distributions for PMT-B

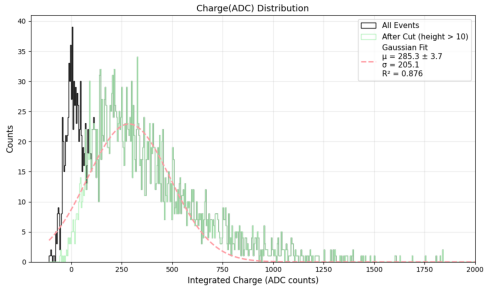

(a) PMT-B at the top position

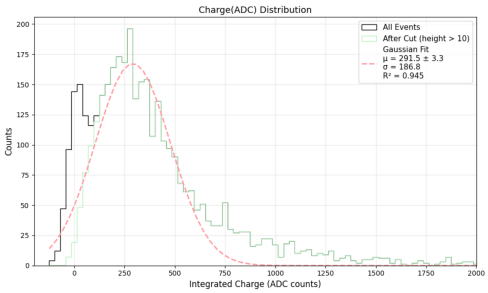

(b) PMT-B at the bottom position

Figure 13: Integrated ADC distributions for PMT-B under different positional configurations in pure water.

B Additional Charge Distributions for Top-PMTs comparison

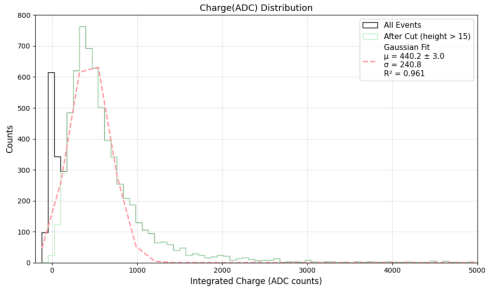

(a) PMT-A at the top position in WbLS

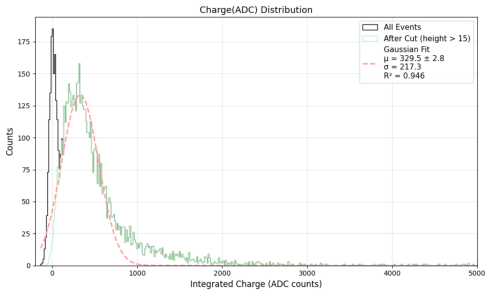

(b) PMT-A at the top position in pure water

Figure 14: Integrated ADC distributions for PMT-A in WbLS and pure water.

References

An, F., An, G., An, Q., Antonelli, V., Baussan, E., Beacom, J., Bezrukov, L., Blyth, S., Brugnera, R., Avanzini, M. B., Busto, J., Cabrera, A., Cai, H., Cai, X., Cammi, A., Cao, G., Cao, J., Chang, Y., Chen, S., ... Zou, J. (2016). Neutrino physics with juno. *Journal of Physics G: Nuclear and Particle Physics*, *43*(3), 030401. https://doi.org/10.1088/0954-3899/43/3/030401

Díaz, J. L., Dobarro, A., Villacampa, B., & Velasco, D. (2001). Structure and optical properties of 2,3,7,9-polysubstituted carbazole derivatives. experimental and theoretical studies. *Chemistry of Materials*, *13*(8), 2528–2536. https://doi.org/10.1021/cm001218n

Fukuda, S., Fukuda, Y., Hayakawa, T., Ichihara, E., Ishitsuka, M., Itow, Y., Kajita, T., Kameda, J., Kaneyuki, K., Kasuga, S., Kobayashi, K., Kobayashi, Y., Koshio, Y., Miura, M., Moriyama, S., Nakahata, M., Nakayama, S., Namba, T., Obayashi, Y., ... Kobayashi, H. (2003). The super-kamiokande detector. *Nuclear Instruments and Methods in Physics Research Section A: Accelerators, Spectrometers, Detectors and Associated Equipment*, *501*(2), 418–462. https://doi.org/https://doi.org/10.1016/S0168-9002(03)00425-X

Onda, N., Asano, Y., Iida, T., Kikawa, T., Nakaya, T., Tokiyasu, A., & Wakabayashi, D. (2025). Development and performance evaluation of a water-based liquid scintillator tracking detector with wavelength-shifting fiber readout. https://arxiv.org/abs/2507.18893

Xiang, X., Yang, G., Andrade, S., Askins, M., Asner, D. M., Baldoni, A., Cowen, D., Diwan, M. V., Gokhale, S., Hans, S., Jerome, J., Lawley, G., Linden, S., Gann, G. D. O., Reyes, C., Rosero, R., Seberg, N., Smiley, M., Speece-Moyer, N., ... Yeh, M. (2024). Design, construction, and operation of a 1-ton water-based liquid scintillator detector at brookhaven national laboratory. https://arxiv.org/abs/2403.13231

Yeh, M., Hans, S., Beriguete, W., Rosero, R., Hu, L., Hahn, R., Diwan, M., Jaffe, D., Kettell, S., & Littenberg, L. (2011). A new water-based liquid scintillator and potential applications. *Nuclear Instruments and Methods in Physics Research Section A: Accelerators, Spectrometers, Detectors and Associated Equipment*, *660*(1), 51–56. https://doi.org/https://doi.org/10.1016/j.nima.2011.08.040